



# Investigation on single crystal by tartaric acid–barium chloride: growth and characterization of novel NLO materials

S SHANMUGAN<sup>1</sup> , N SARAVANAN<sup>2</sup>, V CHITHAMBARAM<sup>3,\*</sup>, B DEEPANRAJ<sup>4</sup> and GEETHA PALANI<sup>3</sup>

<sup>1</sup>Research Center for Solar Energy, Department of Physics, Koneru Lakshmaiah Education Foundation, Green Fields, Vaddeswaram 522502, India

<sup>2</sup>Physics Department, Adhiparasakthi College of Engineering, Kalavai 632506, India

<sup>3</sup>Research Centre Physics, Dhanalakshmi College of Engineering, Chennai 601301, India

<sup>4</sup>Department of Mechanical Engineering, Jyothi Engineering College, Thrissur 679531, India

\*Author for correspondence (chithambaramv@gmail.com)

MS received 5 March 2020; accepted 20 May 2020; published online 12 August 2020

**Abstract.** The progress of single crystal followed by C<sub>4</sub>H<sub>6</sub>O<sub>6</sub> (tartaric acid) and BaCl<sub>2</sub> (barium chloride) (TABC; third-order nonlinear optics semi-organic) was synthesized with slow evaporation method using distilled water at room temperature. TABC single crystal was introduced into various characterizations like X-ray diffraction to determine inter atomic cell parameter values. The samples are crystalline structure of monoclinic, which have space group of P<sub>2</sub>. The functional groups of the current material are identified using FT-IR spectrum. Optical parameters like transparency, energy bandgap and Urbach energy have been determined using UV–vis–NIR spectrum. The thermal stability of the material was investigated by differential scanning calorimeter analysis. The mechanical property was studied using Vickers microhardness test. The surface morphology of the material was determined by scanning electron microscope technique. The change in dielectric behaviour of TABC with respect to the function of frequency at various temperatures has been keenly absorbed and discussed. The third-order nonlinear optical parameters were measured using Z-scan analyses.

**Keywords.** Optical material; XRD; microhardness; thermal study; Z-scan analyses.

## 1. Introduction

Third-order nonlinear optical materials have wide applications like optical communication, sensing, signal processing, data storages, optical logic gates, laser radiation protection and THz-wave generation [1–5]. In recent years, a broad investigation was performed to develop the nonlinear optical materials with high extensive applications in photonic and optoelectronic fields. Various studies dealing with organic, inorganic and semiorganic crystals for nonlinear optics have been reported. Semiorganic nonlinear optical materials play an important role in technological industry. In literature many of these materials has been reported. The organic materials possess poor mechanical, thermal properties with high nonlinear optical coefficient. The development of bulky single crystal is very tough for device fabrications. An inorganic material has admirable thermal, optical and mechanical properties of rather nonlinearity owing to the absence of electron– $\pi$  conjugation [6–10]. Nowadays, interest has been made to grow the semiorganic crystals with less delinquency, high laser damage threshold, exceptional mechanical and thermal properties, low angular sensitivity, wide optical transparency, which makes

the material comfortable for device fabrications [11–13]. Lakshmi *et al* [14] studied nonlinear optical materials of *N,N*-diphenylbenzamide (NNDPB) and 4-fluoro-*N,N*-diphenylbenzamide (FNNDPB). The NNDPB and FNNDPB crystals studied using UV–vis–near IR spectra showed results of 100% in the visible area. It is thermally stable up to 483 and 503 K. Second-harmonic generation (SHG) productivity was calculated by the Kurtz–Perry powder method, which is 1.55 and 1.7 times as that of potassium dihydrogen phosphate. Prabukanthan *et al* [15] have analysed *N*-methyl-4-nitrobenzamide, *N*-methyl-*N*-(4-nitrophenyl)benzamide, 4-fluoro-*N*-methyl-*N*-(4-nitrophenyl)benzamide and 4-methoxy-*N*-methyl-*N*-(4-nitrophenyl)benzamide single crystals through the slow evaporation solution progress. In these crystal structures, thermal analysis was 570 K and the efficiency of SHG was 2.25 times higher than the potassium dihydrogen phosphate (KDP) crystal.

L-tartaric acid is a prominent organic nonlinear optical material. In this study, we report tartaric acid barium chloride (TABC), a third-order nonlinear optical, samples studied by solution growth technique. TABC single crystal was introduced into various characterizations like X-ray

diffraction (XRD) to calculate the unit cell lattice parameters values. The different functional groups have been identified by FT-IR spectral analysis and the optical transparency was studied by UV spectral analysis. The bandgap energy and Urbach energy values were calculated from UV absorption profile. Differential scanning calorimeter (DSC) and Vickers hardness studies confirmed that the material has optimum thermal stability and soft material category. Surface morphology was identified by scanning electron microscope (SEM) analyses, and dielectric studies have been performed with different temperatures and frequency to study the electrical response of the material. SHG results exhibit that TABC single crystal is more efficient than the KDP crystal. Z-scan analysis was carried out to find the third-order nonlinear optical parameters.

## 2. Materials and experimental methodology

### 2.1 Synthesis of materials

L-tartaric acid and barium chloride have been synthesized through 1:1 stoichiometric relation. Using triple distilled water, L-tartaric acid was first dissolved, then quantity of the barium chloride is mixed in tartaric acid by constant stirring. We have given the explanation of the result at ambient temperature, later it was followed by slow evaporation technique to obtain single crystals. In order to improve the purity of the synthesized salt, successive recrystallization process was carried out.

### 2.2 Crystal development

Figure 1 shows TABC single crystal grown from saturated aqueous solution under slow evaporation technique. At room temperature (32°C), saturated solution was prepared by using recrystallized salt. The Whatman filter paper of pore size 11  $\mu\text{m}$  was used to filter the solution. The filtered TABC saturated solution was transferred to the beaker with the perforated lid to maintain the rate of evaporation placed



**Figure 1.** Photograph of grown TABC crystal.

at room temperature for crystallization. By slow evaporation technique, the TABC single crystals were harvested after 26 days.

## 3. Characterization studies

### 3.1 Single crystal XRD analysis

The synthesized material is subjected to single crystal XRD studies using BRUKER KAPPA APEX II CCD single crystal XRD instrument. The crystal belongs to monoclinic system with non-centrosymmetric space group  $P_2$ . The unit cell parameter values are  $a = 6.74 \text{ \AA}$ ,  $b = 10.95 \text{ \AA}$ ,  $c = 7.16 \text{ \AA}$ ,  $\alpha = 90^\circ$ ,  $\beta = 91^\circ$ ,  $\gamma = 99^\circ$  and  $V = 528 \text{ \AA}^3$ . These results confirmed that the title compound is one of the elementary and essential material requirements for SHG activity.

### 3.2 FT-IR spectral studies

The interaction between infrared light with matter is a study of infrared spectroscopy. This analysis is very sensitive to the occurrence of different functional group in a material. The Fourier transform infrared (FT-IR) spectral study is based on the fact that the molecules with frequencies of some local vibrations in the range of  $4000\text{--}400 \text{ cm}^{-1}$  using PERKIN ELMER instrument, employed with technique of KBr pellet. The recorded spectrum is shown in figure 2. The infrared radiation when interact with the molecules of compounds, the part of radiations can be absorbed by the molecules and it causes rotation or vibration based on the functional group. FT-IR studies offer details about the molecular structure and chemical bonding of the materials. The peaks around  $3379 \text{ cm}^{-1}$  is ascribed to symmetric and asymmetric  $\text{--OH}$  stretching of water and it is clearly described that of some water molecules mixed with the crystal. The stretching of  $\text{--OH}$  frequency appeared at  $2500 \text{ cm}^{-1}$ . The  $\text{--C--O--}$  group occurrence is indicated by the presence of sharp and intense peak at  $1568 \text{ cm}^{-1}$ , and  $1423 \text{ cm}^{-1}$  peak shows asymmetric  $\text{--C--H}$  bending. The  $\text{--O--CH}$  stretching mode appears at the peak  $1301 \text{ cm}^{-1}$ . The peak absorption at  $1131 \text{ cm}^{-1}$  is due to  $\text{--O--H}$  bending, while  $\text{--C--OH}$  vibration stretching represents the  $\text{--C--OH}$  coordinate group. The peak around  $1068 \text{ cm}^{-1}$  indicates the stretching of  $\text{C--O}$ . The sharp peaks absorbed at  $901 \text{ cm}^{-1}$  represent that  $\text{C--O}$  stretching bond in alcohol  $\text{--C--OH}$  group. The peaks absorbed below  $878 \text{ cm}^{-1}$  are due to stretching vibrations of metal oxygen.

### 3.3 Study of optical functional

A structure with molecular information can be obtained from the UV-vis-NIR spectrum, as the UV and visible light absorption involves the promotion of electrons from  $\sigma$  and  $\pi$  orbitals from lower order state to higher order states.

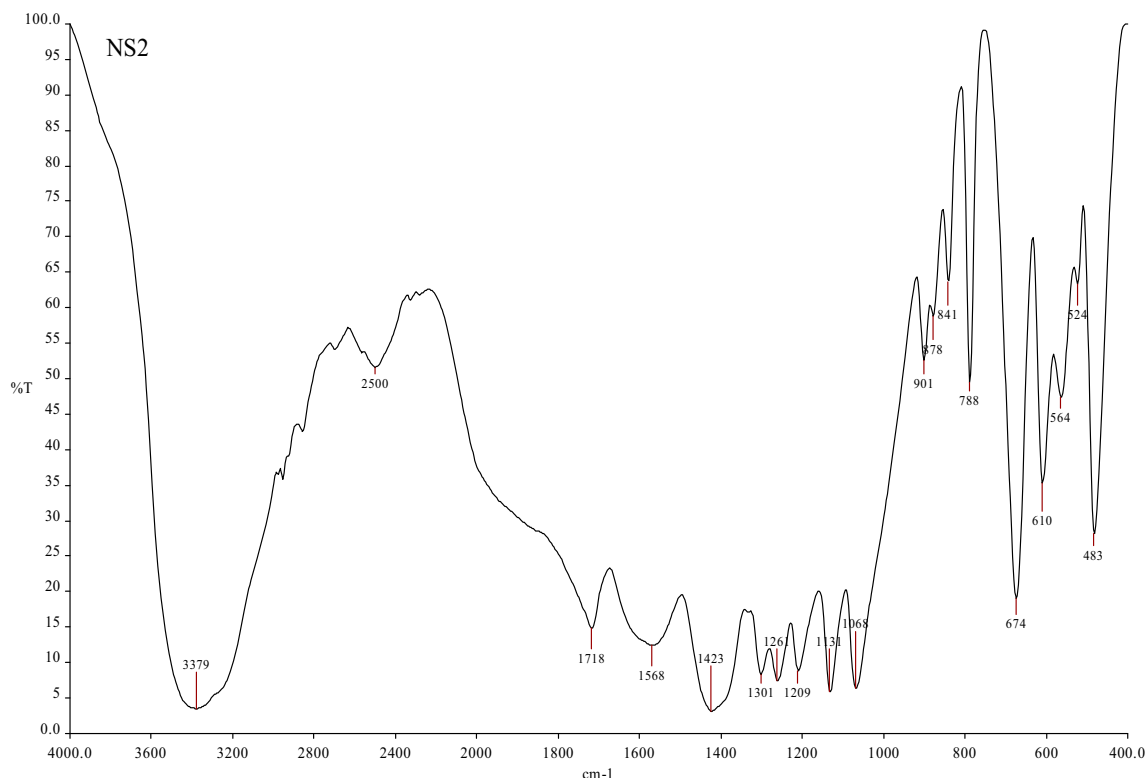


Figure 2. FT-IR spectrum of TABC crystal.

Figure 3 shows the recorded transmittance spectrum of grown crystal in the range of 200–1100 nm using Varian carry 5E spectrophotometer. For the optical applications two factors are very important, such as optical transmittance range and transparency cut-off value [16]. The grown material has lower cut-off value of 210 nm and there is no significant absorption in the entire visible region, which confirms that the TABC can be considered as suitable candidate for SHG and optoelectronics applications. Optical absorption studies serve as an aid to know the optical bandgap and electronic structure.

3.3a *Bandgap energy*: There is a very adjacent relation between atomic and electronic band structures of the direct optical bandgap of the material and it invents applications in electro-optical field. The absorption coefficient ( $\alpha$ ) for TABC material can be found by tauc’s relation with the wavelength [17]:

$$\alpha = A(h\nu - E_g)^{1/2}/h\nu. \tag{1}$$

A value  $E_g$  for TABC material is deliberated with above relation. Tauc’s plot for  $(\alpha h\nu)^2$  vs.  $h\nu$  was pale estimate, energy range shown in figure 4. Here  $\alpha$  is coefficient of

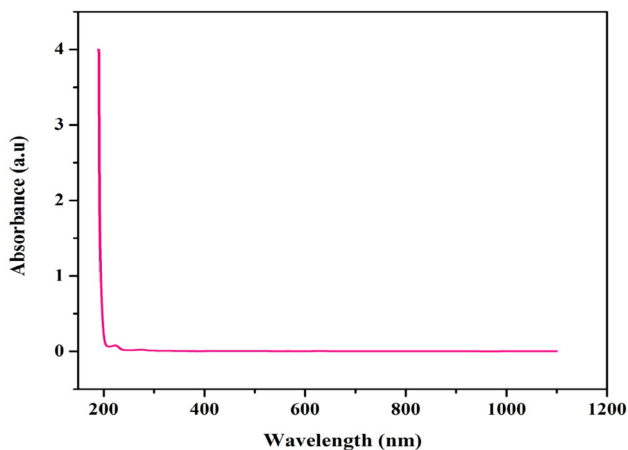


Figure 3. UV-vis spectrum of TABC crystal.

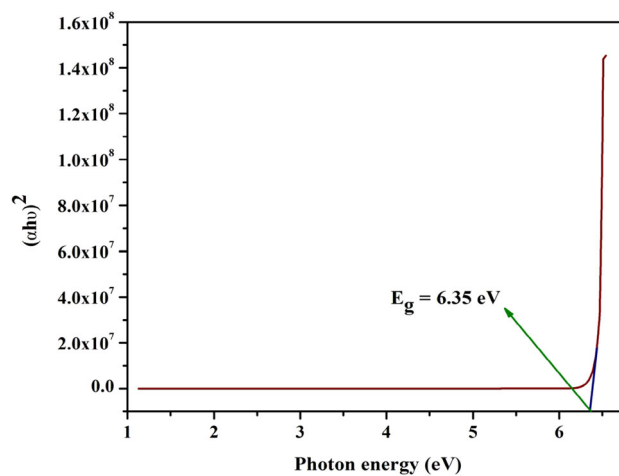


Figure 4. Tauc’s plot of TABC.

absorption,  $h\nu$  is energy photon value (eV) and  $E_g$  is bandgap energy. Value of  $E_g$  in TABC is determined from the slope whose value is 6.35 eV. Such varied photosensitive material is well-suited applicant for laser optical applications.

**3.3b Urbach energy:** Urbach tail is an exponential fragment which lies in the edge of optical band, also in the curve of absorption coefficient [17]. This exponential train appears with those materials having restricted circumstances. The Urbach rule is the product of energy photon ( $h\nu$ ) and absorption coefficient ( $\alpha$ ), with the energy of photon having low range and it is shown in relation:

$$\alpha(h\nu) = \alpha_0 \exp(h\nu/E_u). \quad (2)$$

Here  $E_u$  is Urbach energy or band tail and  $\alpha_0$  is a constant, which is dependent upon the temperature. 'h' is the Planck's constant and 'v' the frequency of radiation. The plot between log absorption coefficients ( $\alpha$ ) with photon energy is shown in figure 5. From the linear portion of the plot, the slope value is found to be 17.3490. Urbach energy is measured as 0.0576 eV from the inverse of direct slice of the plane. These computed low values of Urbach energy (0.0576 eV) confirm that TABC crystal has less structural defect concentrations and it enhances the brilliant nonlinear optical applications.

### 3.4 SEM analysis

The surface nature of the material and its aptness for the device fabrication is confirmed from SEM analysis. These studies also determined the imperfections, if any, present. The surface morphology of the material is reported due to the effectiveness of different impurities [18]. SEM pictures of TABC crystal was obtained using HITACHI S4800, shown in figure 6, with focusing of 2  $\mu\text{m}$ . The various sizes of regular smooth surfaces with number of layers like

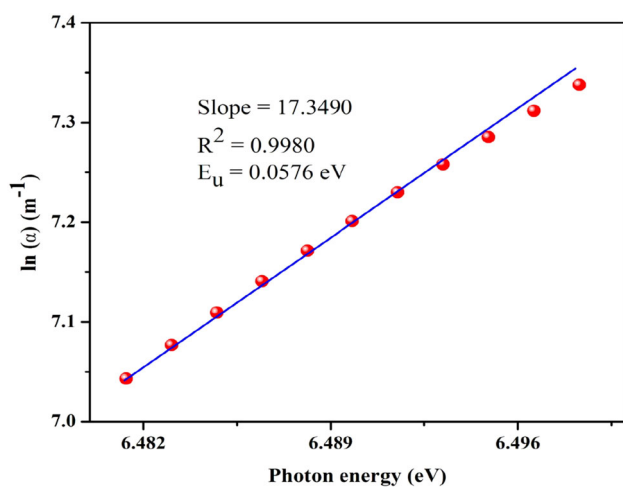


**Figure 5.** Plot  $\ln(\alpha)$  vs.  $h\nu$  for TABC.

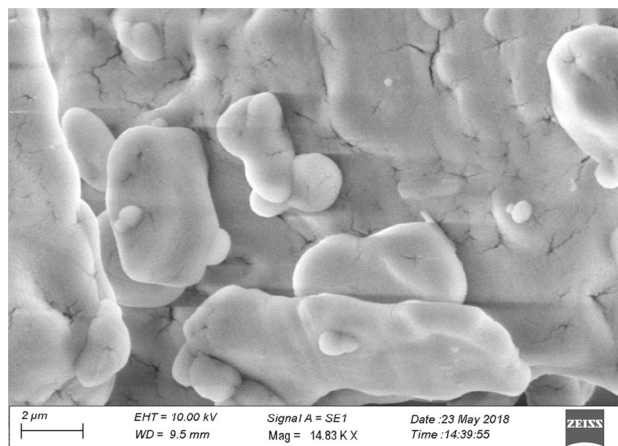


**Figure 6.** SEM image of grown crystal.

pattern, homogenous dispersion of fine grain boundaries on the hierarchies are shown in the SEM pictures. The novel single crystal material size and surface smoothness clearly suggest that TABC crystals play an important role in optoelectronic devices.

### 3.5 Kurtz–Perry powder SHG extent

The SHG efficiency for TABC crystal was determined using modified technique of Kurtz–Perry powder setup. The grown crystals were powdered and gently crowded with micro-capillary uniform tube, which is illuminated with Q-switched Nd:YAG laser radiations, whose fundamental wavelength is 1064 nm. The pulse width of light radiation emitted from the laser source is 8 ns and 1.9 mJ of pulse energy and 10 Hz repetition rate. By the emission of green light radiation (532 nm), SHG was confirmed [19]. For this analysis, the reference sample used is KDP crystal and the grown TABC is 0.6 times greater than that of KDP. A few reported semiorganic crystals are drawn in comparison with the grown crystal, some of them are L-alanine lithium chloride, L-alanine, L-arginine chloride and L-alanine acetate having the SHG efficacy at 0.43, 0.2, 0.2 and 0.30 individually.

### 3.6 DSC analysis

The thermal investigation for grown TABC material was carried using DSC by NETZSCH STA 409C tool in the temperature range of 50–300°C, with the heating rate of 10°C min<sup>-1</sup> in nitrogen atmosphere. The material was taken in the alumina crucible. The obtained DSC curve is depicted in figure 7. The sharp exothermic peak at 83.1°C indicates the melting point of the material. There is no significant phase transition involved until the material melts, indicating that the crystal has extensive temperature range which is very essential for laser applications. During synthesis, the

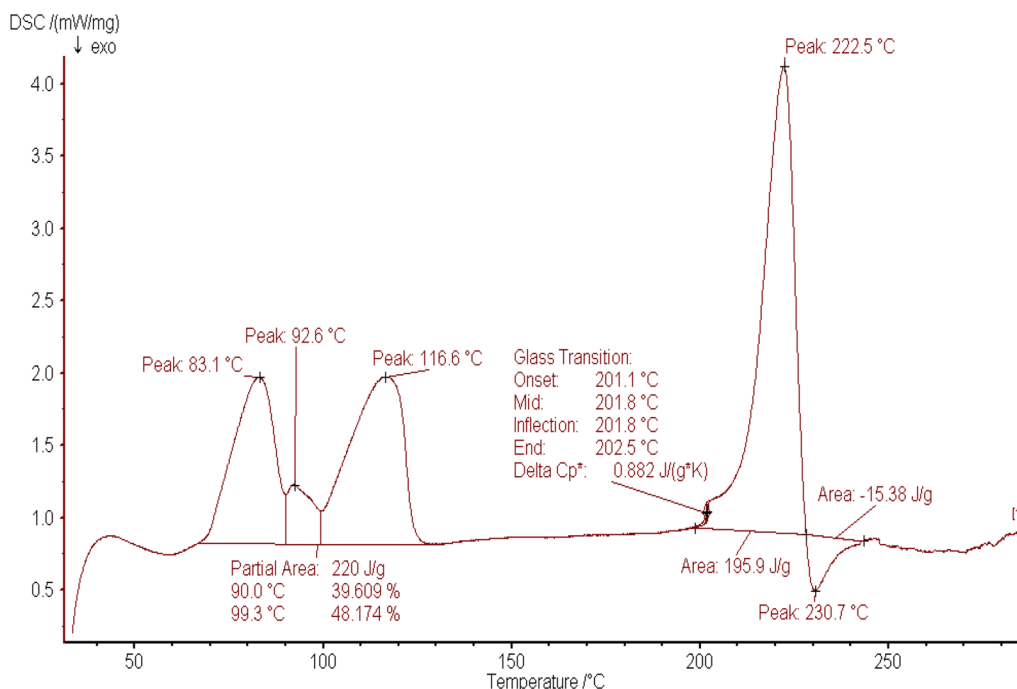


Figure 7. DSC thermal analysis.

water deficiency is noted indicating that the weight loss is absent near 80°C and also near the melting point no decomposition occurred [20]. The exothermic peaks indicate that the material is decomposed totally and volatilized at 92.6 and 116.6°C. At 222.5°C, the material undergoes total decomposition and enhances the range of temperature for crystal ability. This confirms that the material is highly suitable for optoelectronic applications at high temperature.

### 3.7 Dielectric analysis

The electrical response of TABC crystal can be found by using HIOKI 3532-50 LCR HITESTER metre. Using diamond saw the grown crystals were cut and well-polished with paraffin oil. It is coated on either side with silver paint to make the crystal as a capacitor. Now the crystal acts as dielectric material:

$$\epsilon' = \frac{Ct}{A\epsilon_0} \tag{3}$$

From the above relation, dielectric constant is determined with capacitance ‘C’, thickness ‘t’, area ‘A’ of the material and absolute permittivity of the free space  $\epsilon_0$  ( $8.854 \times 10^{-12}$  F m<sup>-1</sup>). The dielectric constant ( $\epsilon'$ ) of TABC can be obtained with frequency by different temperatures viz., 313, 333, 353, 373 K, as shown in figure 8. The high dielectric constant value with less frequency is the contributions of different types of polarizations. The *vice-versa* is mainly by gradual loss of magnitude for all such polarizations [21]. The corresponding graphs are plotted in figures 8 and 9. The low dielectric losses at high frequency

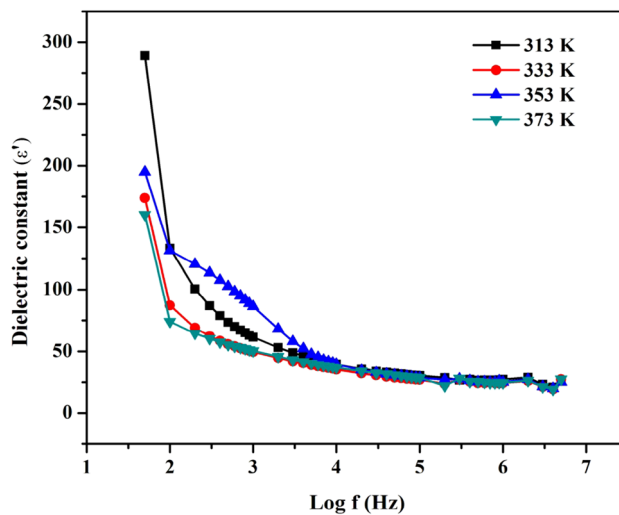


Figure 8. Plot of log frequency vs. dielectric constant of TABC.

advert that the crystal holds prominent optical quality and less defect concentrations. Hence it will be suitable for nonlinear optical applications.

### 3.8 Microhardness studies

The hardness of TABC material was studied using Vickers’s microhardness instrument. Molecular binding, strength and resistance are some parameters of the material collected from the microhardness studies. The value of microhardness correlated with other mechanical properties like yield

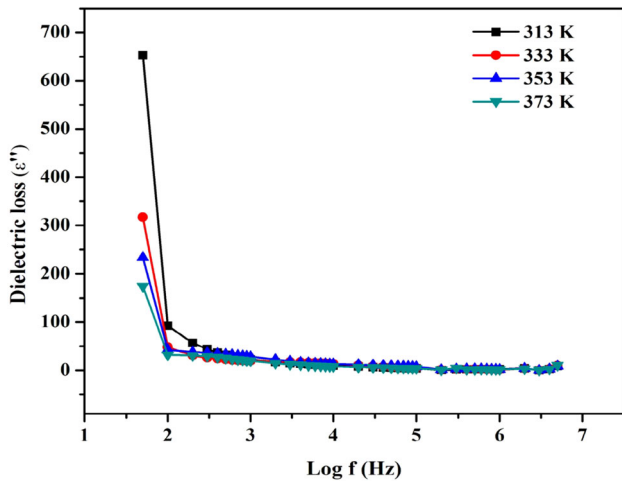


Figure 9. Plot of log frequency vs. dielectric loss of TABC.

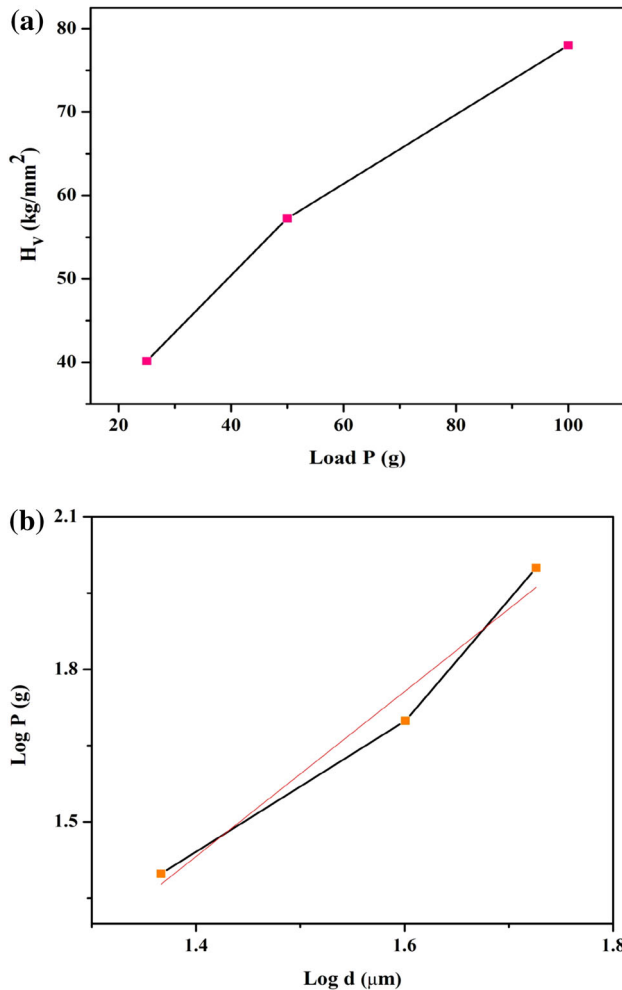


Figure 10. (a) Variation of  $H_v$  with load  $P$ . (b) Plot of  $\log P$  with  $\log d$  for TABC.

strength and elastic constant. The hardness of the material was tested with various load impinge on the surface of the crystal over the indentation time of 10 ns. Figure 10a

illustrates diagram planned amid the consignment ( $P$ ) taken in the  $x$ -axis and hardness ( $H_v$ ) in the  $y$ -axis. From the graph it is observed that the hardness value starts increasing with increase in the load, it depended on the bonding structure if pressure increases, the hardness value decreases. The material withstands the strength up to 100 g. Beyond the 100 g load, cracks were formed on the surface of the crystal [22]. Therefore, the title material can be used only below the load limit of 100 g. The Vickers microhardness value is found to be as follows:

$$H_v = 1.8544(P/d^2) \text{ kg mm}^{-2}. \tag{4}$$

Here ' $P$ ' is load in g and ' $d$ ' the average indentation in mm, and 1.8544 is a constant. In figure 10a, it is well-known that the value of  $H_v$  increases with increase in the load, which underlines reverse indentation size effect (RISE). Hardness of the materials decreases due to the release of stress by increasing the load applied at different indent.

*Mayer index (n):* The Meyer's coefficient was determined by Meyer's law as given by:

$$P = k_1 d^n \tag{5}$$

or

$$\text{Log } P = \text{log } k_1 + n \text{ log } d, \tag{6}$$

where  $k_1$  is the constant and ' $n$ ' Meyer's index, it suggests the material type. Diagram is designed amid  $\log P$  vs.  $\log d$ , as shown in figure 10b. Value of ' $n$ ' is found to be 1.8460 from the slope. The value  $n < 2$  for normal indentation size effect virtue,  $n > 2$  for RISE virtue. According to Onitsch [23], ' $n$ ' represents work hardening coefficient value, 1 and 1.6 for harder materials and more than 1.6 for soft materials. The grown TABC crystal having work hardening coefficient value ' $n$ ' is 1.8460; it promptly shows TABC is under soft material type. Therefore, these materials are considered as suitable candidate for laser damage threshold and device fabrications.

### 3.9 Z-scan studies

The optical parameters like refractive index ( $n_0$ ), absorption coefficient ( $\beta$ ) and third-order optical susceptibility ( $\chi^{(3)}$ ) was carried out using Z-scan analysis, which is one of the prominent tools. The modes of aperture like closed and open in Z-scan experiment can appraise refractive index and absorption property—nonlinear, respectively [24]. The nonlinear absorption property exhibits two categories, such as (i) saturation absorption (SA)—the optical intensity increases with increase in the sample transmittance and (ii) reverse saturation absorption (RSA)—the optical intensity increases with decrease in the sample transmittance. The experiment was performed by CW Nd:YAG laser having 532 nm diode pumps. The light from laser source has the

focus of 15.84  $\mu\text{m}$  and 1.48 mm Rayleigh's length. The optical cell with 1 mm spacious cell containing TABC in dimethylformamide is translate diagonally, that indicates the way for light beam of laser reproduction. At the focal point ( $Z = 0$ ) infer high intensity of absorption saturation. The substance absorbed with multi photon, which is lowest focus (valley) transmittance and highest transmittance for steerable absorption of the substance at focus (peak). The peaks of closed aperture, open aperture for TABC crystals are represented in figure 11a and b. The sign of the non-linear refraction is negative (self-defocusing effect) by valley intensity in the aperture closed, shown in figure 11a [25]. The absorption by the sample is saturated and found in the pattern of open aperture, shown in figure 11b. The computable ( $\Delta T_{P-V}$ ) is measured with  $T_P - T_V$  as function  $\Delta\phi_0$  is

$$\Delta T_{P-V} = 0.406(1 - S)^{0.25} |\Delta\phi_0|, \quad (7)$$

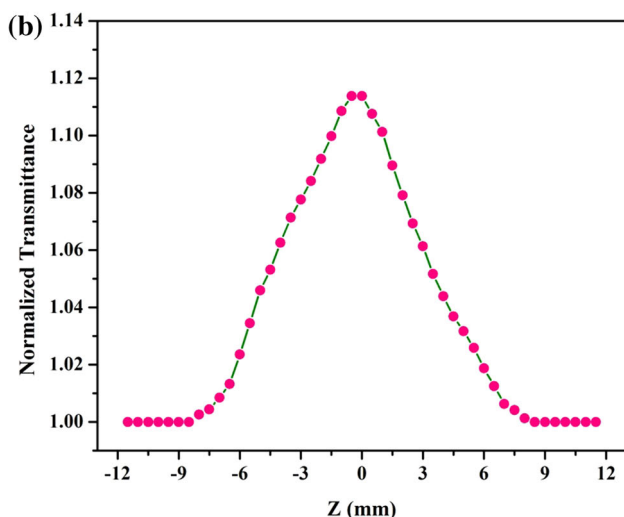
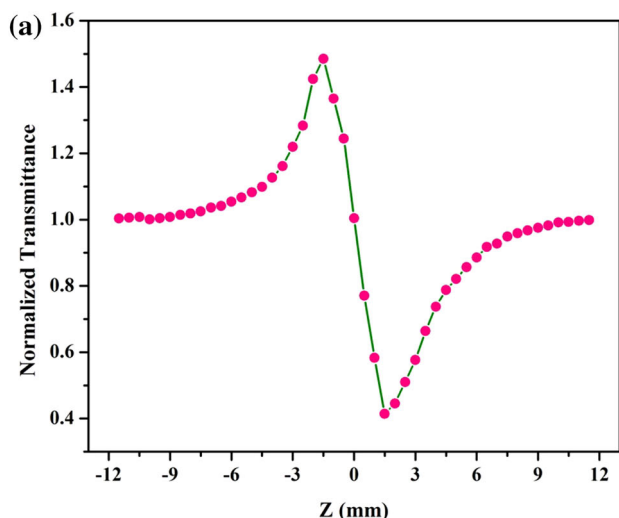


**Figure 11.** (a) Closed aperture and (b) open aperture Z-scan curves.

$$S = 1 - \exp\left(\frac{-2r_a^2}{\omega_a^2}\right), \quad (8)$$

where  $\Delta\Phi_0$  is phase shift, 'S' represents linear opening transmittance,  $r_a$  is aperture radius and  $\omega_a$  is laser spot aperture radius. The relation of  $|\Delta\Phi_0|$  with nonlinear refractive index of third order is given by

$$n_2 = \frac{|\Delta\phi_0|}{kI_0L_{\text{eff}}}\alpha \quad (9)$$

where  $L_{\text{eff}}$  is material breadth,  $I_0$  indicates the intensity, ' $\alpha$ ' the absorption coefficient and ' $k$ ' represents wavenumber. From the curve of open aperture, we determine the non-linear absorption coefficient ( $\beta$ ) using relation:

$$\beta = \frac{2\sqrt{2}\Delta T}{I_0L_{\text{eff}}}. \quad (10)$$

The real part and imaginary part of optical susceptibility can be found using intended values of  $\beta$ ,  $n_2$  by using the relation:

$$\text{Re}\chi^{(3)}(\text{esu}) = \frac{10^{-4}(\epsilon_0 C^2 n_0^2 n_2)}{\pi} \left(\frac{\text{cm}^2}{\text{W}}\right) \quad (11)$$

$$\text{Im}\chi^{(3)}(\text{esu}) = \frac{10^{-2}(\epsilon_0 C^2 n_0 \lambda \beta)}{4\pi^2} \left(\frac{\text{cm}^2}{\text{W}}\right) \quad (12)$$

$\chi^{(3)}$  value be estimated by

$$|\chi^{(3)}| = \sqrt{(\text{Re}(\chi^{(3)}))^2 + (\text{Im}(\chi^{(3)}))^2}. \quad (13)$$

Table 1 illustrates the result and measurable parameter values of Z-scan analysis for TABC material. For the anticipation of visual harm in the direction of high insightful sensors and eyes, these materials possess probable nonlinear optical device applications.

**Table 1.** Nonlinear optical parameters from Z-scan analyses for TABC.

Parameters	Determined values for TABC crystal
Laser beam wavelength ( $\lambda$ )	532 nm
Linear absorption coefficient ( $\alpha$ )	0.0304
Nonlinear refractive index ( $n_2$ )	$4.88 \times 10^{-8} \text{ cm}^2 \text{ W}^{-1}$
Nonlinear absorption coefficient ( $\beta$ )	$0.08 \times 10^{-4} \text{ cm W}^{-1}$
Real part of the third-order susceptibility [ $\text{Re}(\chi^{(3)})$ ]	$2.68 \times 10^{-6} \text{ esu}$
Imaginary part of the third-order susceptibility [ $\text{Im}(\chi^{(3)})$ ]	$0.50 \times 10^{-6} \text{ esu}$
Third-order nonlinear optical susceptibility ( $\chi^{(3)}$ )	$2.77 \times 10^{-6} \text{ esu}$

#### 4. Conclusions

Optically transparent TABC crystal has been obtained by slow evaporation solution growth technique at room temperature. Unit cell parameters were determined from single crystal XRD. The presence of barium chloride in the crystal lattice of tartaric acid was confirmed by FT-IR spectral analyses. Optical analysis concludes, the crystal has low value of cut-off wavelength at 210 nm. Using this optical study,  $E_g$  and Urbach energy ideals are deliberated. SEM study reveals the surface morphology of the grown crystal. SHG efficiency was greater than the reference sample studied using Kurtz–Perry powder test. The thermal studies show that the material possesses optimum thermal stability. The electrical behaviour of grown material was studied using dielectric analysis. The mechanical property was studied by Vickers microhardness test, which shows that material belongs to soft material type. The third-order nonlinear parameters were studied by Z-scan experiment. From the above criteria, we report that TABC material is prominent budding runner for the invention of optoelectronic campaign.

#### References

- [1] Zhang C, Li Z, Cong H, Wang J, Zhang H and Boughton R I 2010 *J. Alloys Compd.* **507** 335
- [2] Arjunan S, Bhaskaran A, Mohan Kumar R, Mohan R and Jayavel R 2010 *J. Alloys Compd.* **506** 784
- [3] Uthrakumar R, Vesta C, Bhagavannarayana G, Robert R and Jerome Das S 2011 *J. Alloys Compd.* **509** 2343
- [4] Chithambaram V and Krishnan S 2014 *Optics Laser Tech.* **55** 18
- [5] Dhanaraj P V, Rajesh N P and Bhagavannarayana G 2010 *Physica B: Condens. Matter* **405** 3441
- [6] Shakir M, Riscob B, Maurya K K, Ganesh V, Wahab M A and Bhagavannarayana G 2010 *J. Cryst. Growth* **312** 3171
- [7] Sonal D, Gupta Ranjith S, Pradhan A, Maeano D, Melikechi N and Desai C F 2002 *J. Appl. Phys.* **91** 3125
- [8] Jiang M H and Fang Q 1999 *Adv. Mater.* **11** 1147
- [9] Oliver S A 2000 *Appl. Phys. Lett.* **76** 3612
- [10] Ramajothi J, Dhanuskodi S and Nagarajan K 2004 *Cryst. Res. Technol.* **39** 414
- [11] Ariponnammal S, Radhika S, Selva R and Victor Jeya N 2005 *Cryst. Res. Technol.* **40** 786
- [12] Linet J M, Dinakaran S and Das S J 2011 *J. Alloys Compd.* **509** 3832
- [13] Dennis J and Henisch H K 1967 *J. Electrochem. Soc. USA* **114** 263
- [14] Lakshmi R, Prabukanthan P, Harichandran G and Kumar C S 2019 *Cryst. Res. Technol.* **54** 1700146
- [15] Prabukanthan P, Lakshmi R, Harichandran G and Kumar C S 2018 *J. Mol. Struct.* **1156** 62
- [16] Chithambaram V, Jerome Das S, Arivudai Nambi R, Srinivasan K and Krishnan S 2010 *Physica B* **405** 2605
- [17] Jayaprakash P, Peer Mohamed M, Krishnan P, Nageshwari M, Mani G and Lydia Caroline M 2016 *Physica B* **503** 25
- [18] Vivekanandhan R, Raju K, Ravisankar V and Chithambaram V 2017 *J. Pure Appl. Math.* **115** 281
- [19] Kurtz S K and Perry T T 1968 *J. Appl. Phys.* **39** 3798
- [20] Saravanan N, Santhanakrishnan S, Suresh S, Sahaya Jude Dhas S, Jayaprakash P and Chithambaram V 2018 *J. Mater. Sci.: Mater. Electron.* **29** 18449
- [21] Chithambaram V, Jerome Das P and Krishnan S 2011 *J. Alloys Compd.* **509** 4543
- [22] Saravanan N, Chithambaram V and Ravisankar V 2018 *J. Mater. Sci.* **29** 5009
- [23] Onitsch E M 1947 *Mikroskopie* **2** 131
- [24] Vijayalakshmi A, Vidyavathy B, Peramaiyan G and Vinitha G 2016 *J. Solid State Chem.* **4596** 30463
- [25] Dhanaraj P V, Rajesh N P, Kalyana Sundar J, Natarajan S and Vinitha G 2011 *Mater. Chem. Phys.* **129** 457